Cys-diabody Quantum Dot Conjugates (ImmunoQdots) for Cancer Marker Detection

Bhaswati Barat,[†] Shannon J. Sirk,[†] Katelyn E. McCabe,[†] Jianqing Li,[‡] Eric J. Lepin,[†] Roland Remenyi,[§]
Ai Leen Koh,[§] Tove Olafsen,[†] Sanjiv S. Gambhir,[ǁ] Shimon Weiss,[‡] and Anna M. Wu*,[†]

Crump Institute for Molecular Imaging, Department of Molecular and Medical Pharmacology, David Geffen School of Medicine
at UCLA, 570 Westwood Plaza, Los Angeles, California 90095, Department of Chemistry and Biochemistry, University of
California, 607 Charles E. Young Drive East, Los Angeles, California 90095, Materials Science and Engineering Department,
Stanford University, Stanford, California 94305, and Molecular Imaging Program at Stanford (MIPS), Department of Radiology
and Department of Bioengineering, Stanford University, 300 Pasteur Drive, Stanford, California 94305. Received
October 1, 2008; Revised Manuscript Received June 12, 2009

The present work demonstrates the use of small bivalent engineered antibody fragments, cys-diabodies, for biological
modification of nanoscale particles such as quantum dots (Qdots) for detection of target antigens. Novel
bioconjugated quantum dots known as immunoQdots (iQdots) were developed by thiol-specific oriented coupling
of tumor specific cys-diabodies, at a position away from the antigen binding site to amino PEG CdSe/ZnS Qdots.
Initially, amino PEG Qdot 655 were coupled with reduced anti-HER2 cys-diabody by amine-sulfhydryl-reactive
linker [N-ε-maleimidocaproyloxy] succinimide ester (EMCS) to produce anti-HER2 iQdot 655. Spectral
characterization of the conjugate revealed that the spectrum was symmetrical and essentially identical to
unconjugated Qdot. Specific receptor binding activity of anti-HER2 iQdot 655 was confirmed by flow cytometry
on HER2 positive and negative cells. Immunofluorescence results showed homogeneous surface labeling of the
cell membrane with Qdot 655 conjugate. In addition, cys-diabodies specific for HER2, as well as prostate stem
cell antigen (PSCA), were conjugated successfully with amino PEG Qdot 800. All of these iQdots retain the
photoluminescence properties of the unconjugated Qdot 800 as well as the antigen binding specificity of the
cys-diabody as demonstrated by flow cytometry. Simultaneous detection of two tumor antigens on LNCaP/PSCA
prostate cancer cells (which express PSCA and HER2) in culture was possible using two iQdots, anti-HER2
iQdot 655 and anti-PSCA iQdot 800. Thus, these iQdots are potentially useful as optical probes for sensitive,
multiplexed detection of surface markers on tumor cells. The present thiol-specific conjugation method demonstrates
a general approach for site-specific oriented coupling of cys-diabodies to a wide variety of nanoparticles without
disturbing the antigen binding site and maintaining small size compared to intact antibody.

INTRODUCTION

In recent years, optical imaging has emerged as a sensitive
detection method for diagnostic and therapeutic purposes.
Quantum dots (Qdots), nanometer-scale semiconductor materi-
als, represent an important class of fluorescent probe for
biomolecular and cellular imaging (1). Qdots are promising as
optical probes because they exhibit high quantum yields, are
resistant to photobleaching, have narrow and size-tunable
emission wavelengths, and have broad excitation spectra. These
unique optical properties of Qdots make them appealing as *in
vivo* and *in vitro* fluorophores in a variety of biological
investigations. Furthermore, since the emission wavelength is
readily tuned by controlling the size of the Qdots, they can be
synthesized to emit different colors, allowing multiplex imaging,
which is increasingly important in the analysis of complex
biological systems (2). The use of Qdots as optical probes was
originally pioneered by Alivisatos and Weiss and by Nie, in

1998. In the investigations of Alivisatos et al., two different-
sized CdSe-CdS core−shell nanocrystals enclosed in a silica
shell were prepared for fluorescent imaging of mouse fibroblast
cells (3). Nie et al. investigated receptor mediated endocytosis
of transferrin receptor in cultured HeLa cells using CdSe-ZnS
Qdots coupled with transferrin (4). By chemically conjugating
antibodies and peptides to their surface, quantum dots can
specifically target cellular ligands of interest. Biocompatible
Qdots have thus been applied for labeling cells (fixed and live)
and tissues (5−7), long-term cell trafficking (8), multicolor cell
imaging (9), tumor cell extravasation tracking (10, 11), fluo-
rescence resonance energy transfer (FRET)-based sensing (12),
bioluminescence resonance energy transfer (BRET)-based imag-
ing (13), and sentinel lymph-node mapping (14). In addition,
semiconductor Qdots have been shown to be suitable for real-
time *in vivo* imaging and Qdots surface-modified with poly-
(ethylene glycol) (PEG) were reported to be biocompatible for
in vivo cancer targeting and imaging (15−17).

Antibodies can be engineered into a wide variety of formats
that retain binding specificity with target antigen and exhibit
optimal properties such as rapid targeting and controlled blood
clearance for *in vitro* or *in vivo* applications (18, 19). Intact
monoclonal antibodies are large (150 kDa) protein molecules.
For coupling to Qdots, smaller antibody fragments would be
preferable to intact IgGs (Figure 1A); otherwise, the overall size
of the antibody−Qdot conjugate becomes quite large. Smaller
antibody fragments have been shown to be superior in their

* Author to whom correspondence should be addressed. Anna M.
Wu, Crump Institute for Molecular Imaging, Department of Molecular
and Medical Pharmacology, David Geffen School of Medicine at
UCLA, 570 Westwood Plaza, CNSI 4335, Los Angeles, CA 90095,
USA. Tel: 310 794 5088; Fax: 310 206 8975; E-mail: awu@
mednet.ucla.edu.
† David Geffen School of Medicine at UCLA.
‡ Department of Chemistry and Biochemistry, University of California.
§ Materials Science and Engineering Department, Stanford University.
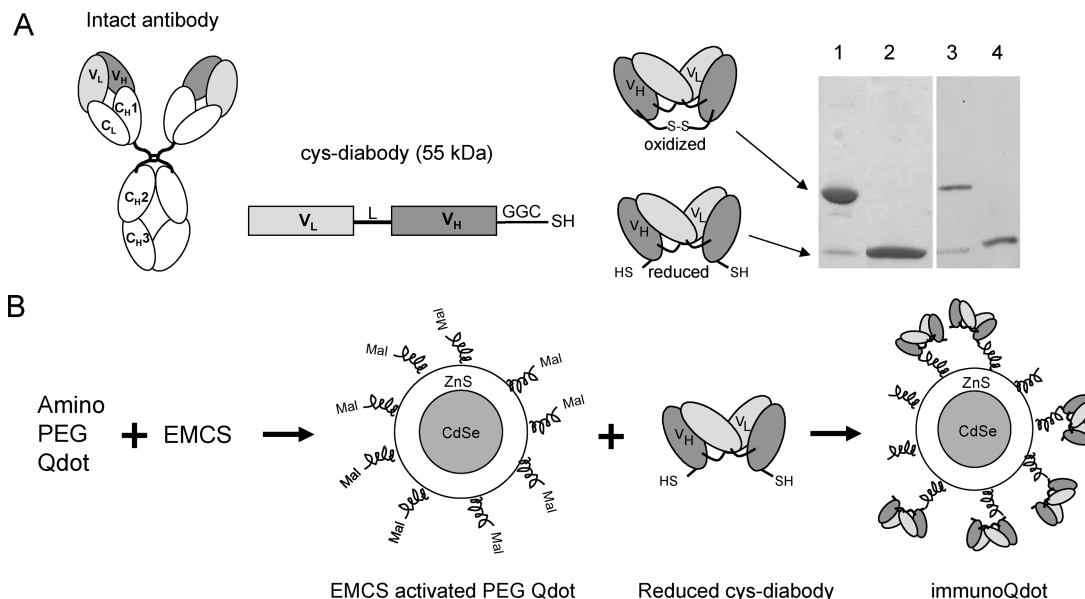ǁ Molecular Imaging Program at Stanford.

Figure 1. (A) Schematic drawing of an intact antibody showing variable light (V_L) and heavy (V_H) chain regions and constant (C) regions. Cys-diabody was formed by connecting V_L and V_H domains with either 5 or 6 amino acid linker (L) and GGC added to the C-termini for cysteine modification. DNA construct and oxidized and reduced forms of protein are shown. SDS-PAGE of two cys-diabodies: lanes 1 and 2, oxidized and reduced forms of anti-HER2 cys-diabody; 3 and 4, oxidized and reduced forms of anti-PSCA cys-diabody. Nonreduced samples migrate at expected size for covalent dimer (50 kDa), and reduced samples migrate at expected size for monomeric scFv (25 kDa). (B) Schematic illustration of the process of conjugating amino PEG Qdot with cys-diabody. EMCS: [*N*-ε-Maleimidocaproyloxy] succinimide ester. Mal: maleimide group.

ability to extravasate and penetrate solid tumors *in vivo*, when compared with intact antibodies (*20*). Genetically fusing the variable light (V_L) and heavy (V_H) chain domains of a parental antibody through a peptide linker results in the production of a single-chain variable fragments (scFv, 27 kDa), at about 1/6 the size of native antibody, with the same specificity as that of parental intact antibody. Shortening the peptide linker results in formation of noncovalent dimers of scFvs, called diabodies (Db, 55 kDa) which retain full antigen binding activity and specificity in smaller formats (*21*). Our lab has previously demonstrated that radiolabeled diabodies against cell surface cancer antigens efficiently target tumors *in vivo* by microPET (*22, 23*). Their small size (5 × 7 nm) makes these engineered antibody fragments specifically appropriate for conjugation to nanoscale particles.

Conjugation by random chemical modification may be risky for small antibody fragments, due to the possibility of inadvertently disrupting the binding site. Site-specific conjugation is more likely to preserve the binding activity of an antibody. X-ray crystallographic structure of the anti-CEA T84.66 diabody shows that the C-termini of the diabody subunits are almost 70 Å apart and on an alternate face from the antigen-combining site (*24*). Introduction of cysteine residues at the C-termini of scFv fragment has been considered as an approach to allow site-specific, thiol-reactive coupling at a site away from the antigen binding site to a wide variety of agents (Figure 1A) (*25−28*). Previous work from our laboratory demonstrated site-specific conjugation and radiolabeling of an anti-CEA diabody with C-terminal cysteine (cys-diabody) for rapid tumor targeting and imaging in CEA-positive xenograft bearing mouse by microPET (*26*).

Numerous studies indicate that the avidity effect of having more than one binding site improves the targeting and retention of antibodies and immunoconjugates. For eventual *in vivo* delivery, an antibody-nanoparticle conjugate needs to be small but also bivalent. Use of a bivalent cys-diabody as the targeting moiety ensures that (at least) two binding sites are attached to the particle, and optimization should allow production of 1:1 conjugates. In contrast, in order to achieve bivalency using

monovalent scFv fragments, titration and optimization will be more challenging and yields probably lower, since a broad distribution of conjugation ratios, including monovalent complexes, will be obtained.

The present study demonstrates oriented site-specific coupling of bivalent cys-diabodies specific for well-characterized cancer cell surface antigens, HER2 and prostate stem cell antigen (PSCA) to fluorescent semiconductor amino PEG Qdots using thiol chemistry. Cys-diabody conjugated Qdots are termed immunoQdots (iQdots). Initial biophysical and functional characterization was performed with anti-HER2 iQdot 655. This iQdot demonstrated dual functionality: retention of HER2 antigen binding specificity as well as fluorescence signal of Qdot. Using two iQdots, anti-HER2 iQdot 655 and anti-PSCA iQdot 800, simultaneous detection of two antigens, HER2 and PSCA, on LNCaP/PSCA cells can be possible by *in vitro* optical imaging. This study allows a general approach for biological modification of a variety of nanoscale particles with small bivalent engineered antibody fragments in an oriented fashion without affecting the antigen binding site and maintaining the overall small size compared to intact antibody.

EXPERIMENTAL PROCEDURES

Design, Expression and Purification of Cys-diabodies. The anti-HER2 cys-diabody was constructed from trastuzumab (Herceptin; Genentech, San Francisco, CA) human variable regions using an existing single-chain variable fragment (scFv) gene construct as template (*29*). Affinity matured recombinant scFv fragment, derived from humanized anti-PSCA antibody (hu1G8 mAb) (*30*) was used as a template for anti-PSCA cys-diabody (Lepin, E. unpublished data). Overlap-extension PCR and site-directed mutagenesis (QuickChange XL, Stratagene, La Jolla, CA) were used to generate both of the cys-diabody constructs with the following orientation: V_L-linker-V_H-C-terminal cysteine modification (GGC) (*28*). 5-Amino acid linker, SGGGG, and 6-amino acid linker, SGGGGS, are the linkers used to construct anti-HER2 and anti-PSCA cys-diabodies, respectively. The final PCR product of anti-HER2 cys-diabody was cloned in the pEE12 mammalian expression vector (Lonza

Biologics, Slough, UK) (*28*) containing a mammalian leader sequence for secretion. The anti-PSCA cys diabody was cloned into pSyn1 plasmid for bacterial expression (gift of Dr. James D. Marks, University of California, San Francisco) (*31*).

For expression of anti-HER2 cys-diabody, 2.5×10^6 NS0 cells (*32*) were transfected by electroporation with 10 μg linearized plasmid DNA and selected in glutamine-deficient media as described (*25*). Anti-HER2 cys-diabody expression was screened by Coomassie stained SDS-PAGE precast 4−20% gels (Bio-Rad, Hercules, CA), under reducing and nonreducing conditions. The highest-expressing clones were expanded into triple flasks (Nunclon, Rochester, NY).

For bacterial expression of the anti-PSCA cys-diabody, *Escherichia coli* BL21 cells transformed with the pSyn1 expression vector were grown in Luria-Bertani broth (LB) to an OD_{600} of 0.7, induced with a final concentration of 1 mM IPTG, and grown for 4 h at 37 °C. Periplasmic extracts were prepared using Peripreps Periplasting Kits (Epicenter, Madison, WI).

Both of the cys-diabodies, anti-HER2 and anti-PSCA, were purified by immobilized protein L chromatography according to the manufacturer's instructions (Pierce, Rockford, IL). The final concentration of the purified proteins was determined by $A_{280 \text{ nm}}$ using an extinction coefficient $\varepsilon = 1.4$. Purified proteins were analyzed by SDS-PAGE under reducing and nonreducing conditions. Cys-diabodies were also subjected to gel filtration chromatography on a Superdex 75 HR 10/30 column (GE Healthcare, Piscataway, NJ). Final protein yields were 3.0 mg/L of mammalian culture supernatant for anti-HER2 cys-diabody and 0.2 mg/L of bacterial culture supernatant for anti-PSCA cys-diabody.

Coupling of Qdots to Tumor-Specific Cys-diabodies. Cys-diabodies were covalently conjugated to Qdot 655 and Qdot 800 amino (PEG) quantum dots (Invitrogen, Carlsbad, CA). Briefly, Qdots were activated with the heterobifunctional cross-linker[*N-ε*-maleimidocaproyloxy] succinimide ester (EMCS) (Pierce) for 30 min at room temperature in 50 mM borate buffer (pH 7.4), yielding a maleimide-modified particle. In each reaction, 60 μg of cys-diabodies were simultaneously reduced by incubating in 20 mM DTT in PBS at room temperature for 30 min. Excess EMCS and DTT were removed using Bio-Spin 6 (Bio-Rad) desalting columns. Mock conjugation controls were also treated under the same conditions, with no cys-diabody added. Then, activated Qdots were incubated with reduced antibody fragment at room temperature for 1 h in 50 mM borate buffer (pH 7.4). The molar ratio of antibody fragment to Qdot was 22:1. The reaction was quenched by adding 34 μg of *N*-ethyl maleimide (NEM, 10 mg/mL in DMSO, Pierce) per mg of antibody fragment. The uncoupled free cys-diabody and excess NEM were removed by three washes using a 100 KDa ultrafiltration unit, Amicon Ultra-4 (Millipore Corp., Bedford, MA). The final iQdot complex was stored in 10 mM borate buffer at 4 °C.

Cell Lines. NS0 mouse myeloma cells (*32*) and human breast cancer cell lines MCF7 (American type Culture Collection [ATCC], Manassas, VA; #HTB-22) transfected with HER2 (MCF7/HER2 (*33*)) were maintained as described (*29*). Human prostate cancer cell lines LNCaP (American type Culture Collection (ATCC; #CRL-1740) transfected with PSCA (LNCaP/PSCA (*34*)) and human B-cell lymphoma cell line SKW 6.4 (ATCC; #TIB-215) transfected with PSCA (SKW6.4/PSCA) (a generous gift of Dr. Robert Reiter, UCLA) were maintained as described (*35*). SK-OV-3, the human ovarian carcinoma cell line (ATCC; #HTB-77) was maintained in McCoy's 5A medium (Mediatech, Inc., Herndon, VA) supplemented with 10% FBS, and Jurkat helper T cell lines (ATCC # TIB-152) were maintained as recommended by ATCC.

Photoluminescence Spectra. The emissions of unconjugated and conjugated Qdot 655 were determined using a QuantaMaster QM-6 steady state spectrofluorometer (Photon Technology International, Inc., Birmingham, NJ) with a 75 W xenon lamp and a 928R PMT. All NIR emission spectra were recorded on a CCD-array based SPM-002 spectrometer (Photon Control Inc., British Columbia, Canada) with a 532 nm diode pumped laser as pumping source.

Flow Cytometry. MCF7/HER2 cells were incubated with either anti-HER2 iQdot 655 or anti-HER2 iQdot 800 for 1 h at 4 °C in PBS containing 1% FBS. LNCaP/PSCA cells were incubated with anti-PSCA iQdot 800 using the same conditions. Approximately 0.83 pmol of Qdots were used in flow cytometry experiments. The cells were then washed with PBS containing 1% FBS. Antibody fragments binding to tumor cells were quantified by FACSCalibur flow cytometer (Becton Dickinson, UK), and data were analyzed using Cell Quest software (Becton Dickinson). FL3 (λ_{em}: 670 nm long pass) and FL5 (λ_{em}: 740 nm long pass) filters were used for Qdot 655 and Qdot 800, respectively.

For competitive cell binding assays, experiments were performed in triplicate on MCF7/HER2 cells by the addition of a fixed concentration of anti-HER2 iQdot 655 (10 nM) and increasing concentrations of anti-HER2 antibody fragment, minibody (*29*) (0.1−1000 nM) as competitor. Binding of anti-HER2 iQdot 655 on cells was examined by flow cytometry. Result was normalized to the signal obtained in the absence of competitor.

Confocal Microscopy. MCF7/HER2 cells were plated on poly(L-lysine)-coated glass coverslips (BD Biosciences, San Jose, CA) in 12-well plates in DMEM medium containing 5% FBS for 24 h. The next day, cells were incubated with mock conjugated Qdot 655 and anti-HER2 iQdot 655 in PBS/1% FBS on ice for 1 h. Approximately 1.7 pmol of Qdots were used in confocal microscopy experiments. Cells were fixed with 3.7% paraformaldehyde at 4 °C for 30 min. Cell nuclei were counterstained with DAPI. Coverslips were mounted on glass slides and observed using a Zeiss LSM510 META confocal imaging system (excitation: argon laser 488 nm) (Carl Zeiss Inc., Thornwood, NY) equipped with a 100× oil immersion objective lens.

Fluorescence Imaging of Qdot Labeled Cells. LNCaP/PSCA cells were incubated with two different iQdots, anti-HER2 iQdot 655 and anti-PSCA iQdot 800 in microfuge tubes. For control experiment, cells were incubated with mock conjugated Qdot 655 and Qdot 800. Cells with Qdots were incubated for 1 h at 4 °C in PBS containing 1% FBS. Approximately 3.3 pmol of Qdots were used in fluorescence imaging experiments. Cells were then washed twice with PBS (1% FBS) to remove any unbound Qdots. Antibody-conjugated Qdots binding to tumor cells were examined using Maestro *In-vivo* Fluorescence Imaging System (CRI, Inc., Woburn, MA) with a blue filter set (excitation, 445−490 nm; emission, 515 nm long-pass, 515−900 nm). CRI software *Maestro 2p23* was used to analyze the data.

RESULTS

Synthesis and Biophysical Characterization of Anti-HER2 iQdot 655. Anti-HER2 cys-diabody was expressed in mammalian cells and purified successfully. Analysis of the purified proteins on SDS-PAGE showed that the cys-diabody migrated as a monomer consistent with its predicted molecular weight of approximately 25 kDa under reducing conditions and as covalent dimer of 55−60 kDa under nonreducing conditions (Figure 1A). An excess amount of reduced cys-diabody was allowed to react with activated amino PEG CdSe/ZnS Qdot 655 using the heterobifunctional cross-linker EMCS to form anti-HER2 iQdot 655 (Figure 1B).
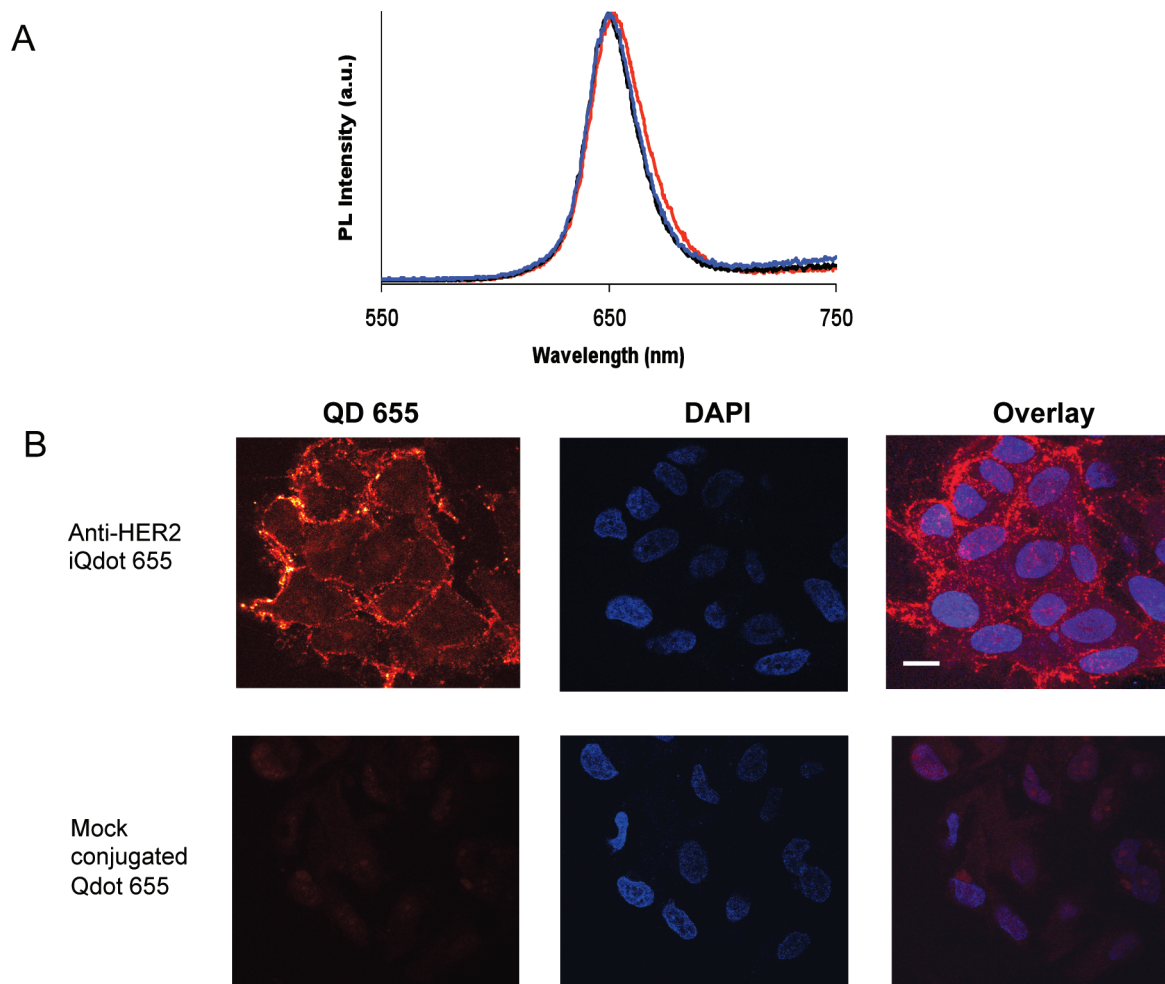
Figure 2. (A) Photoluminescence (emission) spectra of amino PEG Qdot 655 conjugates at excitation wavelength 488 nm. Maximum emission wavelengths are 650.0, 650.5, and 652.5 nm for commercial Qdot 655 (black line), mock conjugated Qdot 655 (blue line), and anti-HER2 iQdot 655 (red line), respectively. All spectra are typically around 30 to 50 nm (full width at half-maximum). (B) Confocal microscopy images of MCF7/HER2 cells stained with anti-HER2 iQdot 655 and mock conjugated Qdot 655. Cell nuclei were counterstained with DAPI and shown in blue. Scale bars: 20 μm.

To visualize the structure of synthesized anti-HER2 iQdot 655, transmission electron microscopy (TEM) was performed on anti-HER2 iQdot 655 and mock conjugated Qdot 655. TEM bright field images revealed that Qdots were uniform in size; prior to and following conjugation, only the inorganic particles are directly visualized at approximately 15 × 5 nm (Supporting Information Figure 1). Negative staining of the conjugates reveals an additional halo, consistent with the conjugation of protein to the particles. Size exclusion chromatography was also performed to evaluate conjugated Qdots. Chromatography on a Superdex 200 HR column showed a single peak eluting at 18.03 min, slightly earlier than that of mock conjugated Qdot 655 (18.28 min) suggesting a relatively uniform preparation without extensive aggregation (Supporting Information Figure 2).

To evaluate whether there was any difference in the photoluminescence (PL) spectrum of Qdots after conjugation to cys-diabody, PL measurements of Qdots were performed by excitation with a 488 nm laser. Figure 2A shows that the spectrum of anti-HER2 iQdot 655 is still symmetrical and almost identical to that of commercial Qdots with only a slight red shift.

Functional Characterization of Anti-HER2 iQdot 655. To determine whether the anti-HER2 iQdot 655 could bind to HER2, HER2 expressing human breast carcinoma MCF7/HER2 cells were incubated with anti-HER2 iQdot 655 and examined by confocal microscopy. The result demonstrated homogeneous surface labeling of the cell membrane with minimal cytoplasmic labeling. Minimal nonspecific binding to the cells was observed with mock conjugated Qdot 655 (Figure 2B).

The anti-HER2 iQdot 655 was also used to assess HER2 expression on MCF7/HER2 cells by flow cytometry. Results showed a strong fluorescent shift of anti-HER2 iQdot 655 with MCF7/HER2 cells (Figure 3A). Control experiments were performed to show the specificity of anti-HER2 iQdot 655. Incubation of MCF7/HER2 cells with mock conjugated Qdot 655 (Figure 3A) or anti-CD20 iQdot 655 (irrelevant iQdot, negative control; data not shown) did not show a shift in fluorescence intensity. Anti-HER2 iQdot 655 also bound efficiently to other HER2 positive cells, i.e., SK-OV-3, ovarian carcinoma cells, and LNCaP/PSCA prostate cancer cells (Figure 3A). No binding was seen to HER2-negative Jurkat cells (Figure 3A).

In order to further evaluate the binding specificity of anti-HER2 iQdot 655, a cell-based competition assay in which Qdot conjugated cys-diabody was incubated simultaneously in the presence of increasing concentrations of competitor, was carried out and analyzed by flow cytometry (Figure 3B). At higher concentrations of the competitor, lower amounts of iQdot were bound. This confirmed that anti-HER2 iQdot 655 retained the same epitope specificity as that of the anti-HER2 antibody fragment.
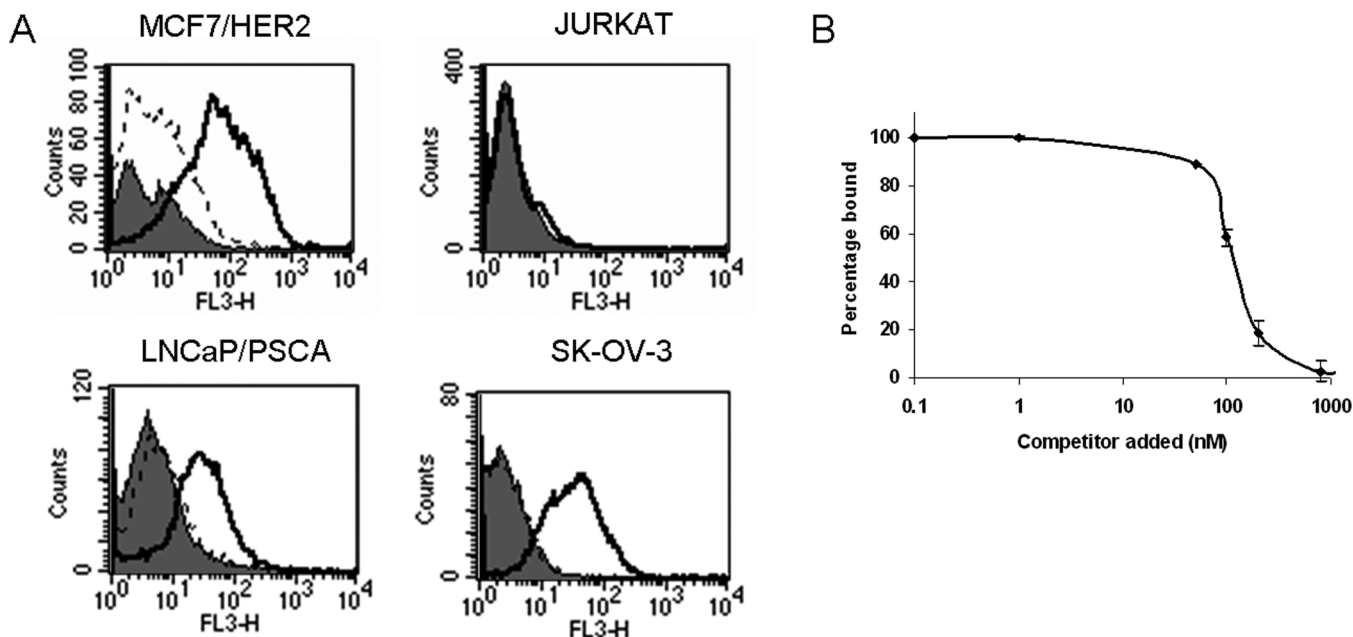
Figure 3. (A) Flow cytometry analysis of cys-diabody conjugated Qdot binding with different tumor cells. Cells were treated with no protein (solid gray), mock conjugated Qdot 655 (dotted black line), and anti-HER2 iQdot 655 (solid black line). FL3 (λ_{em}: 670 nm long pass) was the filter used for Qdot 655. (B) Competitive cell binding assay by flow cytometry. An anti-HER2 antibody fragment, minibody (*29*) was used as competitor. Samples were assayed in triplicate and means ± SEM are shown, normalized to the signal obtained in the absence of competitor.

Functional and Biophysical Characterization of NIR iQdots. In small animals, NIR (700−900 nm) fluorescence imaging is expected to have major utility, because the absorbance spectra for biomolecules reach minima in the NIR region, providing a window for *in vivo* optical imaging. We extended the coupling of anti-HER2 cys-diabody to amino PEG CdSe/ZnS Qdot 800 (emission maximum at 785 nm, anti-HER2 iQdot 800). The specific binding of anti-HER2 iQdot 800 on MCF7/HER2 cells was confirmed by cell binding assay (Figure 4A). In order to demonstrate this oriented thiol-specific coupling of other cys-diabodies specific for cell surface antigens to Qdots, we considered PSCA as an additional target. Applying the same thiol chemistry, we conjugated anti-PSCA cys-diabody with amino PEG Qdot 800 using EMCS (anti-PSCA iQdot 800). Strong binding of anti-PSCA iQdot 800 to LNCaP/PSCA cells was demonstrated by flow cytometry (Figure 4B).

PL measurements of NIR Qdots were performed following excitation with a 532 nm laser. The PL spectra measurements of the Qdots showed maxima at around 785 nm (Figure 4C). There was no significant change observed in mock conjugated and antibody conjugated Qdot spectra.

Duplex Antigen Detection of Prostate Cancer Cells Using Two Colored iQdots. Initially using individual Qdot conjugated cys-diabodies, anti-HER2 iQdot 655 and anti-PSCA iQdot 800, the expression of each target antigen, HER2 and PSCA, was examined on different cancer cells (Table 1). Detection of two individual cancer markers on LNCaP/PSCA prostate cancer cells (which also express HER2) was verified by previous flow cytometry experiments using anti-HER2 iQdot 655 and anti-PSCA iQdot 800 separately (Figure 3A and Figure 4B). Simultaneous detection of the two tumor markers on the same cells was not possible due to lack of proper filters and instrumental settings. To examine the feasibility of multiplex fluorescence imaging, LNCaP/PSCA prostate cancer cells were incubated with two different Qdot conjugates and imaged using a Maestro *In Vivo* optical imaging system (Figure 5A). The spectral analysis shows the presence of two distinct peaks of anti-HER2 iQdot 655 and anti-PSCA iQdot 800 (Figure 5B)

verifying that multiplex fluorescence imaging is possible with these iQdots.

DISCUSSION

In this study, we report the site-specific conjugation of engineered antibody fragments with visible/NIR quantum dots for *in vitro* cell labeling and multiplex imaging. A key feature of this approach is the use of cys-diabodies which represent the smallest bivalent antibody fragment that can be generated from intact antibodies. Furthermore, this cys-diabody format enables site-specific, oriented coupling, ideal for applications in nanotechnology. Initial studies showed that Qdots functionalized with anti-HER2 cys-diabody retained antigen-specific cell binding, demonstrated by flow cytometry and fluorescence microscopy. In addition, utilizing the same technique, anti-PSCA cys-diabody was successfully conjugated to Qdots and two-color analysis was possible. The amine modified quantum dots used in this study include a PEG spacer covalently attached to the Qdot surface. We found that the PEG linker gave less nonspecific background compared to the corresponding carboxyl-modified Qdot 655, which does not possess a PEG linker (unpublished data). This characterization is most likely due to the increased hydrophilicity and higher stability resulting from the PEG-coating. The PEGylation reduces the surface charge and as a result, the nonspecific binding is reduced (*16*).

PEGylated Qdots have been used for *in vivo* imaging in mice (*17*). Addition of multiple PEG molecules provides improved biocompatibility and blood retention time. These improved properties of Qdots can facilitate their use as optical imaging probes *in vivo*. Recently, the delivery of Qdot 655 labeled antibody to tumor cells was investigated by *in vivo* real-time tracking (*11*). RGD modified Qdots have also recently been tracked in vasculature by their binding with integrins using intravital microscopy (*36*). PEGylated commercial Qdots had shown slower uptake into liver and spleen and low-level bone uptake in mice compared to un-PEGylated Qdot (*37*), but overall clearance times were still very rapid (6 min vs 2 min).

Use of engineered antibody fragments with Qdots for detection of a specific organic compound, 2,4,6-trinitrotoluene
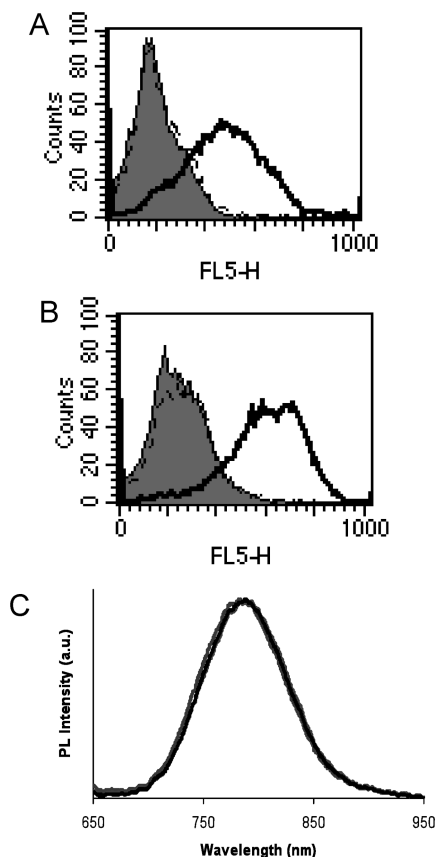
Figure 4. (A) Flow cytometry analysis of cys-diabody conjugated NIR Qdot binding with MCF7/HER2 Cells. Cells were treated with no protein (solid gray), mock conjugated Qdot 800 (dotted black line), and anti-HER2 iQdot 800 (solid black line). (B) LNCaP/PSCA cells stained with no protein (solid gray), mock conjugated Qdot 800 (dotted black line), and anti-PSCA iQdot 800 (solid black line). FL5 (λ_{em}: 740 long pass) was the filter used for Qdot 800. (C) Normalized emission spectra of amino PEG Qdot 800 conjugates. Excitation wavelength was 532 nm. Corresponding emission peaks and associated full-width half-maximum values were 787.9 and 88.95, 785.7 and 89.19, and 789.0 and 89.62 nm for mock conjugated Qdot 655 (black line), anti-HER2 iQdot 800 (red line), and anti-PSCA iQdot 800 (brown line), respectively.

Table 1. Binding Assay of Different ImmunoQdots with Different Tumor Cell Lines

cell line	Anti-HER2 iQdot 655	Anti-PSCA iQdot 800
Jurkat	−	−
MCF7/HER2	+	−
SKW/PSCA	−	+
LNCaP/PSCA	+	+

(TNT) was demonstrated using a scFv fragment (*38*). This study showed the use of luminescent Qdots conjugated to antibody fragments in a solution-phase nanosensor, based on fluorescence resonance energy transfer (FRET) for the specific detection of the explosive TNT in aqueous environments. Attachment of the anti-TNT specific scFv fragments to a hydrophilic Qdot via metal affinity coordination is another example of oriented attachment of small antibody fragments to Qdots. *In vivo* applications may be limited by the size of the overall complexes. In contrast, the present approach to site-specifically label cys-diabodies to any nanoscale particles can be used for *in vitro* as well as *in vivo* applications depending on the size of the conjugated particle.

In contrast to *in vitro* applications, many challenges exist *in vivo*, in particular, when targeting tumor is the goal. Many factors influence the penetration of antibody to areas distal from the blood vessels (*39*). These include antibody affinity, con-
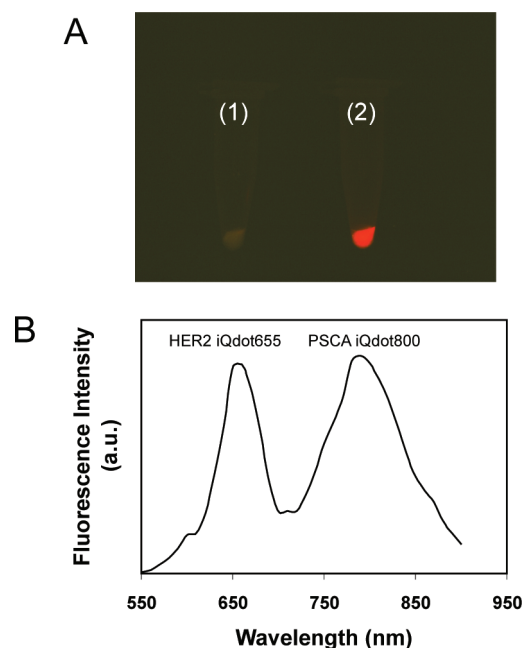

Figure 5. Dual marker Qdot staining of human prostate cancer cells. (A) *In vitro* fluorescence imaging of LNCaP/PSCA cells stained with (1) mock conjugated Qdot 655 and Qdot 800 and (2) anti-HER2 iQdot 655 and anti-PSCA iQdot 800. The raw fluorescence image acquired using a color CCD camera with a 550 to 900 nm filter is shown. (B) Spectral analysis of dual stained cells (sample 2) following background subtraction.

centrations, antibody size, vascular permeability, and intratumoral pressure. Methodologies for introducing specificities onto Qdots by conjugating intact antibodies specific for HER2 antigen and prostate-specific membrane antigen (PSMA) for *in vivo* study have been developed (*11, 17*). In mice bearing PSMA expressing tumor xenografts, in addition to tumor uptake, the antibody conjugated Qdots were trapped in the liver and spleen (*17*).

Previous studies of antibodies and antibody fragments have shown rapid and homogeneous tumor penetration by scFv fragments compared to other immunoglobulin forms (*20*). One potential shortcoming of the current Qdot conjugation strategies with biomolecules, especially vis-à-vis *in vivo* applications, is that the Qdot bioconjugates are quite large (∼40−50 nm) once streptavidin or intact antibodies are incorporated. Such large nanoparticles will have difficulty in traversing the endothelium and penetrating into tissues and tumors. In contrast, if smaller antibody fragments such as cys-diabodies are directly labeled to Qdots, the overall smaller size of these iQdots should be more suitable for *in vivo* applications. Further gains can be made by conjugation to even smaller particles such as zwitterionic, cys-coated quantum dots (QD-Cys) having hydrodynamic diameters of about 5.5 nm for rapid and efficient renal clearance and extravasation (*40*). Schipper et al. have further examined the effects of particle size, surface coating, and PEGylation on the biodistribution and clearance of small, near-infrared InAs Qdots, observing a shift toward renal clearance following PEGylation of the smallest, peptide-coated Qdots (*41*).

In conclusion, cys-diabodies are small, bivalent tumor-targeting antibody fragments that retain antigen binding specificity after incorporation of the cysteine-modification at the C-termini. Their small size and favorable pharmacokinetics make them ideal for use in imaging and therapeutic applications. The present study demonstrates site-specific, oriented conjugation of cys-diabodies to commercially available amino PEG quantum dots. The iQdots retain the photoluminescence properties of the unconjugated Qdots as well as the antigen binding

specificity of the cys-diabody. The overall small size of cys-diabody conjugated Qdots should render them suitable for biological applications. The results of Qdot conjugation to cys-diabodies with different tumor specificities opens up new prospects for multiplex imaging in cancer. This thiol-reactive conjugation approach can be used as a generalized platform for site-specific coupling of cys-diabodies with a wide variety of other nanoparticles, such as quantum rods or carbon nanotubes.

ACKNOWLEDGMENT

Supporting Information Available: Experimental methods and results of TEM images and gel filtration chromatography as described in the text. This material is available free of charge via the Internet at http://pubs.acs.org.

LITERATURE CITED

(1) Michalet, X., Pinaud, F. F., Bentolila, L. A., Tsay, J. M., Doose, S., Li, J. J., Sundaresan, G., Wu, A. M., Gambhir, S. S., and Weiss, S. (2005) Quantum dots for live cells, in vivo imaging, and diagnostics. *Science 307*, 538–44.

(2) Xing, Y., Chaudry, Q., Shen, C., Kong, K. Y., Zhau, H. E., Chung, L. W., Petros, J. A., O'Regan, R. M., Yezhelyev, M. V., Simons, J. W., Wang, M. D., and Nie, S. (2007) Bioconjugated quantum dots for multiplexed and quantitative immunohistochemistry. *Nat. Protoc. 2*, 1152–65.

(3) Bruchez, M., Jr., Moronne, M., Gin, P., Weiss, S., and Alivisatos, A. P. (1998) Semiconductor nanocrystals as fluorescent biological labels. *Science 281*, 2013–6.

(4) Chan, W. C., and Nie, S. (1998) Quantum dot bioconjugates for ultrasensitive nonisotopic detection. *Science 281*, 2016–8.

(5) Fountaine, T. J., Wincovitch, S. M., Geho, D. H., Garfield, S. H., and Pittaluga, S. (2006) Multispectral imaging of clinically relevant cellular targets in tonsil and lymphoid tissue using semiconductor quantum dots. *Mod. Pathol. 19*, 1181–91.

(6) Howarth, M., Takao, K., Hayashi, Y., and Ting, A. Y. (2005) Targeting quantum dots to surface proteins in living cells with biotin ligase. *Proc. Natl. Acad. Sci. U.S.A. 102*, 7583–8.

(7) Wu, X., Liu, H., Liu, J., Haley, K. N., Treadway, J. A., Larson, J. P., Ge, N., Peale, F., and Bruchez, M. P. (2003) Immunofluorescent labeling of cancer marker Her2 and other cellular targets with semiconductor quantum dots. *Nat. Biotechnol. 21*, 41–6.

(8) Stroh, M., Zimmer, J. P., Duda, D. G., Levchenko, T. S., Cohen, K. S., Brown, E. B., Scadden, D. T., Torchilin, V. P., Bawendi, M. G., Fukumura, D., and Jain, R. K. (2005) Quantum dots spectrally distinguish multiple species within the tumor milieu in vivo. *Nat. Med. 11*, 678–82.

(9) Jaiswal, J. K., Mattoussi, H., Mauro, J. M., and Simon, S. M. (2003) Long-term multiple color imaging of live cells using quantum dot bioconjugates. *Nat. Biotechnol. 21*, 47–51.

(10) Voura, E. B., Jaiswal, J. K., Mattoussi, H., and Simon, S. M. (2004) Tracking metastatic tumor cell extravasation with quantum dot nanocrystals and fluorescence emission-scanning microscopy. *Nat. Med. 10*, 993–8.

(11) Tada, H., Higuchi, H., Wanatabe, T. M., and Ohuchi, N. (2007) In vivo real-time tracking of single quantum dots conjugated with monoclonal anti-HER2 antibody in tumors of mice. *Cancer Res. 67*, 1138–44.

(12) Medintz, I. L., Clapp, A. R., Mattoussi, H., Goldman, E. R., Fisher, B., and Mauro, J. M. (2003) Self-assembled nanoscale biosensors based on quantum dot FRET donors. *Nat. Mater. 2*, 630–8.

(13) So, M. K., Xu, C., Loening, A. M., Gambhir, S. S., and Rao, J. (2006) Self-illuminating quantum dot conjugates for in vivo imaging. *Nat. Biotechnol. 24*, 339–43.

(14) Kim, S., Lim, Y. T., Soltesz, E. G., De Grand, A. M., Lee, J., Nakayama, A., Parker, J. A., Mihaljevic, T., Laurence, R. G., Dor, D. M., Cohn, L. H., Bawendi, M. G., and Frangioni, J. V. (2004) Near-infrared fluorescent type II quantum dots for sentinel lymph node mapping. *Nat. Biotechnol. 22*, 93–7.

(15) Maysinger, D., Behrendt, M., Lalancette-Hebert, M., and Kriz, J. (2007) Real-time imaging of astrocyte response to quantum dots: in vivo screening model system for biocompatibility of nanoparticles. *Nano Lett.* n/a.

(16) Ballou, B., Lagerholm, B. C., Ernst, L. A., Bruchez, M. P., and Waggoner, A. S. (2004) Noninvasive imaging of quantum dots in mice. *Bioconjugate Chem. 15*, 79–86.

(17) Gao, X., Cui, Y., Levenson, R. M., Chung, L. W., and Nie, S. (2004) In vivo cancer targeting and imaging with semiconductor quantum dots. *Nat. Biotechnol. 22*, 969–76.

(18) Wu, A. M., and Senter, P. D. (2005) Arming antibodies: prospects and challenges for immunoconjugates. *Nat. Biotechnol. 23*, 1137–46.

(19) Kenanova, V., and Wu, A. M. (2006) Tailoring antibodies for radionuclide delivery. *Expert Opin. Drug Delivery 3*, 53–70.

(20) Yokota, T., Milenic, D. E., Whitlow, M., and Schlom, J. (1992) Rapid tumor penetration of a single-chain Fv and comparison with other immunoglobulin forms. *Cancer Res. 52*, 3402–8.

(21) Holliger, P., Prospero, T., and Winter, G. (1993) "Diabodies": small bivalent and bispecific antibody fragments. *Proc. Natl. Acad. Sci. U.S.A. 90*, 6444–8.

(22) Sundaresan, G., Yazaki, P. J., Shively, J. E., Finn, R. D., Larson, S. M., Raubitschek, A. A., Williams, L. E., Chatziioannou, A. F., Gambhir, S. S., and Wu, A. M. (2003) 124I-labeled engineered anti-CEA minibodies and diabodies allow high-contrast, antigen-specific small-animal PET imaging of xenografts in athymic mice. *J. Nucl. Med. 44*, 1962–9.

(23) Wu, A. M., Williams, L. E., and Zieran, L. (1999) Anti-carcinoembryonic antigen (CEA) diabody for rapid tumor targeting and imaging. *Tumor Targeting 4*, 47–58.

(24) Carmichael, J. A., Power, B. E., Garrett, T. P., Yazaki, P. J., Shively, J. E., Raubischek, A. A., Wu, A. M., and Hudson, P. J. (2003) The crystal structure of an anti-CEA scFv diabody assembled from T84.66 scFvs in V(L)-to-V(H) orientation: implications for diabody flexibility. *J. Mol. Biol. 326*, 341–51.

(25) Li, L., Olafsen, T., Anderson, A. L., Wu, A., Raubitschek, A. A., and Shively, J. E. (2002) Reduction of kidney uptake in radiometal labeled peptide linkers conjugated to recombinant antibody fragments. Site-specific conjugation of DOTA-peptides to a Cys-diabody. *Bioconjugate Chem. 13*, 985–95.

(26) Olafsen, T., Cheung, C. W., Yazaki, P. J., Li, L., Sundaresan, G., Gambhir, S. S., Sherman, M. A., Williams, L. E., Shively, J. E., Raubitschek, A. A., and Wu, A. M. (2004) Covalent disulfide-linked anti-CEA diabody allows site-specific conjugation and radiolabeling for tumor targeting applications. *Protein Eng. Des. Sel. 17*, 21–7.

(27) Albrecht, H., Burke, P. A., Natarajan, A., Xiong, C. Y., Kalicinsky, M., DeNardo, G. L., and DeNardo, S. J. (2004) Production of soluble ScFvs with C-terminal-free thiol for site-specific conjugation or stable dimeric ScFvs on demand. *Bioconjugate Chem. 15*, 16–26.

(28) Sirk, S. J., Olafsen, T., Barat, B., Bauer, K. B., and Wu, A. M. (2008) Site-specific, thiol-mediated conjugation of fluorescent probes to cysteine-modified diabodies targeting CD20 or HER2. *Bioconjugate Chem. 19*, 2527–34.

(29) Olafsen, T., Kenanova, V. E., Sundaresan, G., Anderson, A. L., Crow, D., Yazaki, P. J., Li, L., Press, M. F., Gambhir, S. S.,

Williams, L. E., Wong, J. Y., Raubitschek, A. A., Shively, J. E., and Wu, A. M. (2005) Optimizing radiolabeled engineered anti-p185HER2 antibody fragments for in vivo imaging. *Cancer Res. 65*, 5907–16.

(30) Olafsen, T., Gu, Z., Sherman, M. A., Leyton, J. V., Witkosky, M. E., Shively, J. E., Raubitschek, A. A., Morrison, S. L., Wu, A. M., and Reiter, R. E. (2007) Targeting, imaging, and therapy using a humanized antiprostate stem cell antigen (PSCA) antibody. *J. Immunother. (1997) 30*, 396–405.

(31) Bell-Pedersen, D., Dunlap, J. C., and Loros, J. J. (1996) Distinct cis-acting elements mediate clock, light, and developmental regulation of the Neurospora crassa eas (ccg-2) gene. *Mol. Cell. Biol. 16*, 513–21.

(32) Galfre, G., and Milstein, C. (1981) Preparation of monoclonal antibodies: strategies and procedures. *Methods Enzymol. 73*, 3–46.

(33) Slamon, D. J., Clark, G. M., Wong, S. G., Levin, W. J., Ullrich, A., and McGuire, W. L. (1987) Human breast cancer: correlation of relapse and survival with amplification of the HER-2/neu oncogene. *Science 235*, 177–82.

(34) Gu, Z., Thomas, G., Yamashiro, J., Shintaku, I. P., Dorey, F., Raitano, A., Witte, O. N., Said, J. W., Loda, M., and Reiter, R. E. (2000) Prostate stem cell antigen (PSCA) expression increases with high gleason score, advanced stage and bone metastasis in prostate cancer. *Oncogene 19*, 1288–96.

(35) Leyton, J. V., Olafsen, T., Lepin, E. J., Hahm, S., Bauer, K. B., Reiter, R. E., and Wu, A. M. (2008) Humanized radioiodinated minibody for imaging of prostate stem cell antigen-expressing tumors. *Clin. Cancer Res. 14*, 7488–96.

(36) Smith, B. R., Cheng, Z., De, A., Koh, A. L., Sinclair, R., and Gambhir, S. S. (2008) Real-time intravital imaging of RGD-quantum dot binding to luminal endothelium in mouse tumor neovasculature. *Nano Lett 8*, 2599–606.

(37) Schipper, M. L., Cheng, Z., Lee, S. W., Bentolila, L. A., Iyer, G., Rao, J., Chen, X., Wu, A. M., Weiss, S., and Gambhir, S. S. (2007) MicroPET-based biodistribution of quantum dots in living mice. *J. Nucl. Med. 48*, 1511–8.

(38) Goldman, E. R., Medintz, I. L., Whitley, J. L., Hayhurst, A., Clapp, A. R., Uyeda, H. T., Deschamps, J. R., Lassman, M. E., and Mattoussi, H. (2005) A hybrid quantum dot-antibody fragment fluorescence resonance energy transfer-based TNT sensor. *J. Am. Chem. Soc. 127*, 6744–51.

(39) Fujimori, K., Covell, D. G., Fletcher, J. E., and Weinstein, J. N. (1989) Modeling analysis of the global and microscopic distribution of immunoglobulin G, F(ab')2, and Fab in tumors. *Cancer Res. 49*, 5656–63.

(40) Choi, H. S., Liu, W., Misra, P., Tanaka, E., Zimmer, J. P., Itty Ipe, B., Bawendi, M. G., and Frangioni, J. V. (2007) Renal clearance of quantum dots. *Nat. Biotechnol. 25*, 1165–70.

(41) Schipper, M. L., Iyer, G., Koh, A. L., Cheng, Z., Ebenstein, Y., Aharoni, A., Shay, K., Bentolili, L. A., Li, J., Rao, J., Chen, X., Banin, U., Wu, A. M., Sinclair, R., Weiss, S., and Gambhir, S. S. (2009) Particle size, surface coating, and PEGylation influence the biodistribution of quantum dots in living mice. *Small 5*, 126–134.